Design of Pneumatic Actuators for Driving a Two-Axis PV Solar Tracker under Iraqi Climate Conditions

Mustafa A. Abdul-Hussein
Department of Electromechanical Engineering, University of Technology, Baghdad

Jamal A.-K. Mohammed
Department of Electromechanical Engineering, University of Technology, Baghdad

Wisam E. Abdul-Lateef
Department of Electromechanical Engineering, University of Technology, Baghdad

https://doi.org/10.5109/7236838

出版情報：Evergreen. 11 (3), pp.1870-1881, 2024-09. 九州大学グリーンテクノロジー研究教育センター
バージョン：

Design of Pneumatic Actuators for Driving a Two-Axis PV Solar Tracker under Iraqi Climate Conditions

Mustafa A. Abdul-Hussein*, Jamal A.-K. Mohammed, Wisam E. Abdul-Lateef
Department of Electromechanical Engineering, University of Technology, Baghdad, Iraq

*Author to whom correspondence should be addressed:
E-mail: mustafa.abbas3.142@gmail.com

(Received March 2, 2024: Revised June 2, 2024: Accepted July 28, 2024).

Abstract: Electricity production from solar panels is improved by maximizing their capture of solar radiation by tracking sunlight so that it falls perpendicular to the panels. Pneumatic actuators are useful technology for pointing panels toward the sun. They are an alternative to hydraulic actuators, which are maintenance-intensive, leakable, and require many associated components. Electric actuators are large, not suitable for all conditions, and have a high initial cost. Two pneumatic actuators were employed in this paper to drive a two-axis sun tracker. The proposed tracking method provides wide freedom of movement, greatly simplifies the tracking mechanism, possesses many advantages that come with pneumatics, like reducing consumption, costs, environmental risks and the need for ongoing maintenance. This paper aims to provide a comprehensive design of pneumatic actuators to drive a two-axis solar tracker that operates as efficiently as possible, taking into account the maximum load in the worst possible weather conditions in Iraq. This entails determining the piston cylinder length and inner diameter based on certain input parameters such as stroke, fully extended and retracted lengths, and force of the cylinder, impact angles, and wind speed. To examine the actuators' performance, a MATLAB simulation was run on March 1, 2024, in Baghdad-Iraq, on a typical sunny day. The findings showed that when loaded under the greatest wind speed that can occur, roughly 5.5 m/s based on Iraqi climatic statistics, the proposed tracker operates precisely, steadily, and smoothly. Ultimately, the design procedure used 150 mm length pneumatic cylinders to drive the solar panel. Furthermore, at a static inlet pressure of 2 bar for actuators, it was discovered that actuator 1's cylinder diameter measured 22 mm, whereas actuator 2's measured 28.15 mm. Aligning the pneumatic actuators on two axes improved the efficiency of the solar panel by 66.4% when compared to a fixed panel.

Keywords: pneumatic cylinder; dual-axis tracker; PV panel; pneumatic actuator; wind.

1. Introduction

Recently, sustainability has gained great importance. Users are eager to switch from fossil fuels to renewable energy sources[1] like solar, wind, and others. One increasingly attractive replacement for fossil fuels is solar energy. It is among the purest forms of energy that are accessible on our planet. Solar energy may be harnessed for many applications, including water heating systems[2,3], air heating systems[4,5], crop drying systems[6-8], the generation of electricity[9,10], etc. The need for solar energy equipment has increased recently due to the growing emphasis on clean energy. To meet the increasing demand for electrical energy and achieve sustainability goals, multiple means are used, such as hydro, wind, solar, and environmental energy[9]. Solar-powered equipment is common in commercial, residential, and agricultural environments.

The most prevalent component of this equipment is its solar panel, which uses a solar tracking system[11,12] to self-align the panel with the position of the sun to capture solar energy. These devices need solar tracker actuators installed, which allow the solar panels to be oriented in the best possible way concerning the sun so that they get sunlight throughout the day. When the sun is at a low angle, these actuators assist in efficiently harvesting sunlight.

Actuators for solar tracking systems are crucial; hence their design needs to be carefully considered. Actuators need to provide strong durability capabilities, technical accuracy and control, stability, and smooth integration with solar trackers.

The solar trackers are apparatus that follow the sun's journey across the sky, increasing the quantity of sunlight that reaches the PV cells and increasing their ability to produce power. With the use of a solar tracking system

and a solar panel linear actuator or gear motor, solar panel efficiency may be increased by 30% to 40% as compared to stationary solar panels[11].

Linear or rotary actuators[13], solar controllers, and sensors are commonly used in solar trackers. These actuators achieve good solar tracking.

Actuators are driven by energy sources, which might be electrical current, pneumatic pressure, or hydraulic pressure. They transform energy into motion. It enables users to adjust the angles of PV panels. Single-axis[14-16] and dual-axis[12,17,18] solar tracking systems are two distinct varieties that are based on the different structural degrees of freedom. While the other is made to monitor the sun using two axes that correspond to the azimuth and solar altitude angles, the first one uses the azimuth angle to track the sun on a single axis. Novel designs and technologies for both kinds have been created recently to attain high structural dependability and control precision for the actual performance of these systems. A solar tracker is used to make the device's surface always oriented toward the sun to capture the most energy. There are also many types of mechanical actuators; Linear motors[19,20], DC motors and gearboxes[21,22], and stepper motors[16,23]. There are other actuators for driving the solar tracker, including thermo-mechanical[24], hydraulic[25], and pneumatic[26,27].

The pneumatic actuators have a lot fewer critical points of failure and require a lot less maintenance than earlier tracking-array systems. This lowers the likelihood of failure while cutting installation and total costs. Pneumatic actuators have several advantages over hydraulic actuators[28]. When it comes to the cost of manufacture and resistance to contamination, pneumatic actuators perform better than hydraulic actuators. Furthermore, pneumatic actuator systems are not affected by changes in outside temperature. Since actuator exhaust gases don't need to be collected, fluid pipelines are not required. As the pneumatic systems are almost dry, there's no need for long-term storage. Because of their high weight-to-torque ratio and greater flexibility, pneumatic systems are necessary.

In general, pneumatic actuators have some important properties. They are less expensive and offer an excellent force-to-weight ratio. They exhibit better force control, superior positioning control, and increased precision. In addition, these actuators are safer for workers, better for the environment, and more dependable than hydraulic controllers. Due to air compression, nonlinear dynamics, and parasitic frictional effects, pneumatic system designs are far more complex than those of other systems[29], which have promoted their usage. Pneumatic actuators, often known as artificial muscles, have several applications, including automotive applications[30,31], lifting systems[32,33], tracking systems[27,28], medical instruments[34], and robotics[35], etc.

Powerful and efficient pneumatic actuators can be seamlessly integrated with solar panel tracking systems, creating smooth, precisely controlled motion. Pneumatic actuators provide a cost-effective solution of the solar tracker. The low-duty cycle functioning of the pneumatic tracker allows for reduced maintenance requirements, monitoring energy savings, and the possibility of scalability. The design of the actuators used in the solar tracker should aim to achieve high durability, flexibility, responsiveness, and reliability.

The electricity generation of a solar PV tracking system is greatly affected by its geographical location and weather conditions. To maximize the effectiveness and functionality of solar tracker installations, it is essential to understand and take these elements into account during system design to withstand extreme conditions, site selection, and performance monitoring.

The realism of the design results is affected by the solutions of mathematical equations, hence it is crucial to include the geographic location and climate conditions in the research. The worst case scenarios for these conditions must be taken into account when designing a mechanical system. This includes considering whether the system will be placed on the sea, in the desert, on top buildings, or in an area with surrounding mountains. Every single one of these elements has an impact on the actuator design that can move in tandem with the movement of the sun.

There are many studies in the literature concerned with designing solar trackers driven by different types of actuators. Ergashev and Oshchepkova[36] designed a dual-axis solar tracker, providing system protection against strong winds. The tracker was driven by two electric stepper motors. Chaurasia et al.[37] designed a solar tracking system driven by a hydraulic actuator to provide electric energy of 87.6 kWh/year. They have created the first solar tracking system that uses gravitational energy as a driving force and offers a tracking system that works well in distant areas.

Pneumatically driven actuators provide a great substitute for electric and hydraulic actuators and may operate safely in a wide range of challenging environments, such as wet, hot, and dusty ones.

Successful design and implementation of an automated electro-pneumatic single-axis solar tracker has been accomplished by Baisrum et al.[38] with an error of 2.5º, a dynamic response of 2.08% overshoot, and a steady-state error of 1.25% in the load condition. Dhanya and Gopal[39] modeled and designed a pneumatic actuator to guide a single-axis solar tracker. Fathi et al.[40] designed and implemented a dual-axis solar tracker directed by new multifaceted, highly efficient pneumatic actuators. This tracker provides low-duty-cycle operation, monitoring energy conservation, less maintenance requirements, and scaling possibilities because of its inherent energy storage.

So far, the solar tracking studies reported in all the above literature do not adopt a comprehensive computational method in designing the actuators needed

for driving solar trackers in different locations and climatic conditions. The objective of this work is to offer a comprehensive design of the pneumatic actuators needed to drive a two-axis solar tracker while accounting for the maximum load under Iraq's worst weather conditions, including wind speed and impact angles. In this paper, the internal diameter and stroke length of two pneumatic actuators are designed. All forces and torques acting on the system have been analyzed and calculated using MATLAB simulation software.

2. Methodology

2.1 Construction of solar tracker

The mechanical structure of the solar tracking system, shown in Fig. 1, was designed. The structure of the tracker is made of aluminum. The system has two pneumatic actuators to track the sun. The first actuator "1" tracks the linear vertical movement of the sun from south to north at different angles, from the pillar to the solar panel. The second actuator "2" tracks the horizontal movement of the sun from east to west. It is a linear motion converted into a circular motion to provide 180° of precise tracking. The panel is fixed on a frame mounted on a pillar via a free-moving joint to hold and facilitate vertical movement of the frame and panel assembly. The system would be analyzed and a variety of parameters would be calculated according to the local weather conditions.

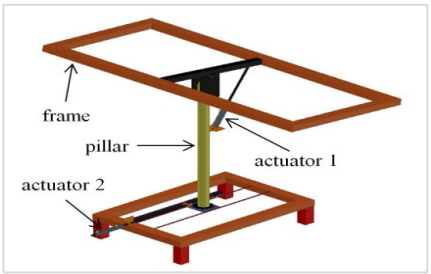

Fig. 1: Scheme of pneumatic solar PV panel tracker

The research methodology depends on performing the following procedures:

– Collecting physical data on the solar panel and pneumatic actuators shown in Fig. 2.

– Using the provided hypothesis to calculate the remaining parameters.

– Producing and evaluating the dual-axis solar tracker using the MATLAB simulation software.

The orientation system is depicted along the rotational axis in Fig. 2.

α_{min} represents the angle produced between the vertical axis (pillar) and the support frame. The rotation system should be designed with α_{min} as the starting tilting angle. The first tilting angle used for the system's symmetry is determined by the sun tracking system's specifications. The range of α_{min} is 0 to $\pi/2$.

To finish the required design, the pneumatic actuator's parameters, stroke D_{str}, fully extended length d_{1max}, fully retracted length d_{1min}, force F, speed, and input voltage, must all be initially determined.

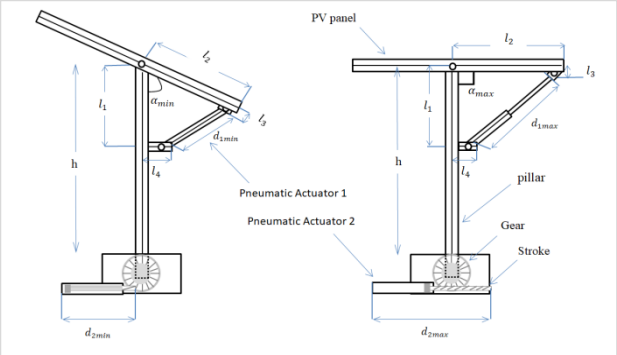

Fig. 2: Orientation with the biggest and smallest rotation angles along the rotation axis.

2.2 Designing the piston length of the pneumatic actuator 1:

To design the pneumatic actuator 1 shown in Fig. 3, the dimensions of the solar panel and the pillar must be taken into account.

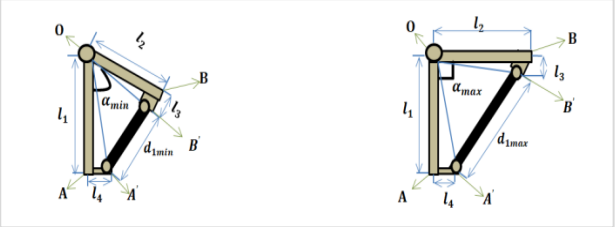

Fig. 3: Dimension calculation model for actuator 1.

This study suggests utilizing a pneumatic actuator mechanism and choosing a calculation technique for this actuator to develop a dual-axis solar tracker for solar panels. A solar PV panel EU-M40W, measuring 670×425×20 mm and weighing 4 kg, is used in this design. The solar panel's area is therefore $a \times b$ = 670×425 mm. The tracker has a pillar with a height h of 730 mm and a circular cross-section with a diameter D_p of 40 mm. The solar panel is mounted using screws on a rectangular aluminum frame with the same dimensions as the panel. The south-north rotation axis of the tracking system is installed at the midpoint of the frame. By defining the lengths of l_1, l_2, l_3, and l_4 illustrated in Fig. 2 and 3, the dimensions of the pneumatic actuator mechanism may be ascertained. l_1 needs to be less than the pillar h's, and l_2 needs to be less than the frame width. To simplify the problem, the following lengths are chosen:

$$l_1 = h/2 = 365\ \text{mm}, l_2 = b/2 = 212.5\ \text{mm}, l_3 = 50\ \text{mm}, \text{and}\ l_4 = 75\ \text{mm} \quad (1)$$

Figure 2 and 3 show the model used for calculating dimensions. The pneumatic actuator's fully extended and retracted lengths may be computed with the model's assistance. The following is an example of how the dimensions relate to one another:

$$OA' = \sqrt{OA^2 + AA'^2},\ OB' = \sqrt{OB^2 + BB'^2},\\ A\hat{O}A' = \text{acrtg}\left(\frac{AA'}{OA}\right), B\hat{O}B' = \text{acrtg}\left(\frac{BB'}{OB}\right) \quad (2)$$

As can be seen in Fig. 3, the values of d_{1min} and d_{1max} are used to calculate the completely expanded and retracted length of the pneumatic actuator, respectively

$$\left.\begin{array}{c} {d_{1\min}}^2 = OA'^2 + OB'^2 - 2OA'.OB' \\ \cos(\alpha_{\min} - A\hat{O}A' - B\hat{O}B') \\ {d_{1\max}}^2 = OA'^2 + OB'^2 - 2OA'.OB' \\ \cos(\pi - \alpha_{\min} - A\hat{O}A' - B\hat{O}B') \end{array}\right\} \quad (3)$$

Depending on the initial minimal tilting angle α_{min}, the values d_{1min} and d_{1max} may be obtained using Eqs. 1, 2, and 3. Figure 3 shows the link between d_{1min} and d_{1max}. The likelihood of receiving sunlight improves with decreasing minimum tilting angle value, and rotational energy correspondingly rises. Assuming that $\pi/3$ is the initial minimum tilting angle, select the pneumatic actuator using the following parameters. $OA' = 373\ \text{mm}, OB' = 221, A\hat{O}A' = 0.2, B\hat{O}B' = 0.2, d_{1\min} = 240\text{mm}, d_{1\max} = 390\text{mm}, D_{str1} = 150\ \text{mm}$, where D_{str1} is the stroke length of pneumatic cylinder piston of actuator 1.

2.3 Designing the cylinder internal diameter of the pneumatic actuator 1:

Several factors must be taken into account when installing a solar tracker, represented by the range of loads that the panel experiences when it rotates, some of which are internal, represented by the weight and size of the panel and its rotating accessories, and some are external, representing the wind load. The wind load affects how close the solar PV panels must be positioned to the roof's edges and exerts excessive stress on the PV modules and PV mounting system, making it a significant consideration. Because friction load is so little, it is ignored in all computations.

Eq. 4 can be used to calculate the actuator 1 force required to move the solar panel vertically.

$$F = [M \times g]_{int\ load} + [\frac{1}{2} \times \rho \times V^2 \times A_w \times C_d]_{wind\ load} \quad (4)$$

Where M in kg is the mass of the tracker's moving parts, C_d denotes the coefficient of wind drag, A_w in m^2 denotes the area of moving parts exposed to the wind, V in m/s is the wind speed, ρ in kg/m^3 represents the air density, and g in m/s^2 is the acceleration due to gravity.

In this case, since the pneumatic actuator 1 is in a lateral position as shown in Fig. 4, the forces must be decomposed into two components and entered into the equation. The lifting force of the actuator can be found as:

$$F = [M \times g \times (\cos(\alpha) + \sin(\alpha))]_{\text{int load}} + [\frac{1}{2} \times \rho \times V^2 \times A_w \times C_d]_{\text{wind load}} \quad (5)$$

Where F in N is the actuator's lifting force and α in rad is the angle of the panel according to the position of the sun. Fig. 4 illustrates the position angle between the panel and the pneumatic actuator 1.

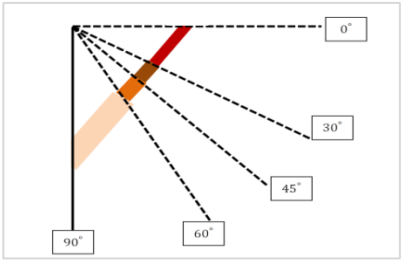

Fig. 4: Angles α between the solar panel and actuator 1.

Then, by changing the angles α in the range from 0 to 90° according to Eq. 5, all the expected forces can be obtained. Figure 5 shows how the lifting force changes with the location of the angle between the vertical axis and the panel. Changing the angle changes the actuator's thrust.

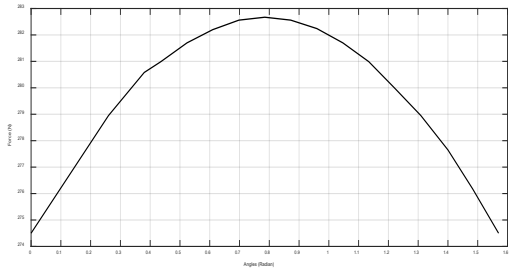

Fig. 5: Analyzing the lifting force of actuator 1 vs. angles.

The nomenclature of the symbols used in the manuscript should be provided as well as their units in the SI system. For example, Spatial analysis of the study of wind speed[41] showed that during the summer, wind speeds increase to 5.5 m/s in the central and southern regions of Iraq due to the flatness of the land surface. When the wind map of Iraq created by the National Renewable Energy Centre of Spain (CENER) was compared to the generated wind map of the yearly average wind speed, a fair resemblance was found[42]. This information was gathered from the Iraq Meteorological Organization and Seismology data that was sent around the country.

The maximum force is adopted for safety design purposes. The highest wind speed in Iraq is taken into account, in addition to adopting an appropriate safety factor. According to Eq. 5 and Fig. 5, the maximum force

will be at an angle of $\pi/4$ (0.7854 rad), so:

$$F_{1(\max)} = [2 \times 9.81 \times (\cos(\pi/4) + \sin(\pi/4))] + [1/2 \times 1.29 \times 5.5^2 \times (0.67 \times 0.425) \times 1.05] = 33.58 \text{ kg.m/s}^2 = 33.58 \text{ N}$$

At the tracking system's center of rotation, the torque of pneumatic actuator 1 is:

$$M_{act1} = F \times [\cos(\alpha) \times l_3 + \sin(\alpha) \times l_2] \quad (6)$$

Figure 6 shows how the variation of the actuator 1 torques with angles.

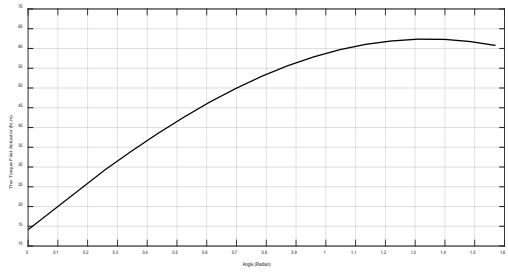

Fig. 6: Torque analysis of pneumatic actuator 1 vs. angles.

According to Eq. 6, the maximum torque will be at an angle of 76.908 (1.3423 rad), so:

$$M_{act1(\max)} = 33.58 \times [\cos(76.908) \times 0.050 + \sin(76.908) \times 0.215] = 7.4 \text{ N.m}$$

After determining the maximum torque value of the pneumatic actuator, the electrical and mechanical parameters of the actuator will be defined. Figure 7 gives an analysis of the moment applied to the center of rotation. Using $m.g.\cos(\alpha)$ as the gravitational force of the panel and the frame, the eccentric moment of the tracking system is given:

$$M_{e1} = m \times g \times \cos(\alpha) \times e \quad (7)$$

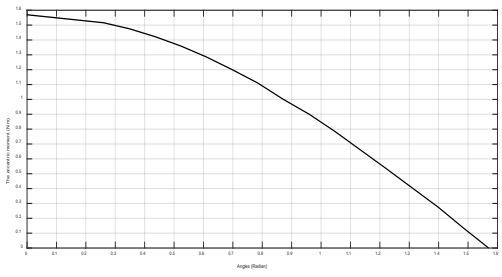

Fig. 7: Eccentric moment analysis of actuator 1 vs. angles.

The maximum value of the eccentric moment of the solar tracker is happening at zero angle.

$$M_{e1(max)} = 4 \times 9.81 \times \cos(0) \times 0.040 = 1.57 \, N.m$$

The eccentricity, or the separation between the panel's center and the system's center of rotation in the direction orthogonal to the panel, is represented by the symbol *e*, where *m* is the solar panel's weight. The moment of the wind relative to the axis of the rotation system is:

$$M_{wind} = C_m \times 0.613 \times V_{(wind)}^2 \times A_w \times b \quad (8)$$

Where *A* (m^2) is the solar panel's surface area, *b* is the solar panel width concerning the rotation axis, V_{wind} (m/s) is the wind speed, and C_m is the coefficient of wind moment according to the angle between the solar panel and wind direction.

Usually, the highest resistance moment is selected to calculate the wind moment M_{wind}, then $C_m = 0.6$[43]. Taking into account the maximum wind speed, which is 5.5 m/s according to Climate Iraqi statistics[41,44], M_{wind} is found to be equal 0.036 N.m according to Eq. 8.

The rotating system's torque balance M_{bal} equation around point *O* is as follows:

$$M_{bal} = M_{act_1} - M_{e_1} - M_{wind} \quad (9)$$

Substituting the values in Eq. 9, yields M_{bal} = 5.767 N.m.

The required pneumatic actuator 1 diameter can be calculated from the force equation:

$$F_1 = P \times A_1 \quad (10)$$

Where A_1 is the area of cylinder 1 and *P* is the air pressure. Using the force value of 2 Bar= $2 \times 10^5 N/m^2 = 2 \times 10^5$ Pascal . Substituting the force and pressure values in Eq. 10, the actuator area A_1 was found as 1.679×10^{-4} m^2. Substituting A_1 in Eq. 11 to find the cylinder diameter of actuator 1:

$$A_1 = \frac{\pi}{4} \times {D_1}^2 \quad (11)$$

Where D_1 is the actuator diameter 1 . So, D_1 = 14.6 mm. Using a safety factor of 1.5, the diameter of the pneumatic cylinder (actuator 1) ≅ 22 mm.

2.4 Designing the cylinder piston length of pneumatic actuator 2

To design the required movement of the pneumatic actuator 2, a gear with a diameter D_g of 90 mm and a chain with a length l_{ch} of 170 mm must be available. The chain must be designed so that it can rotate half the gear. The required chain length l_{ch} was $\pi \times D_g/2$ =142 mm. A 170 mm chain length was chosen for safety design purposes. Therefore, the gear teeth can be fixed in the chain. Increasing the length of the chain does not affect the movement aspect because the main control of the stroke length is the actuator whose length will be designed. The chain must also be mounted on a stabilizer that can move when pushed by the actuator 2, as shown

in Fig. 8.

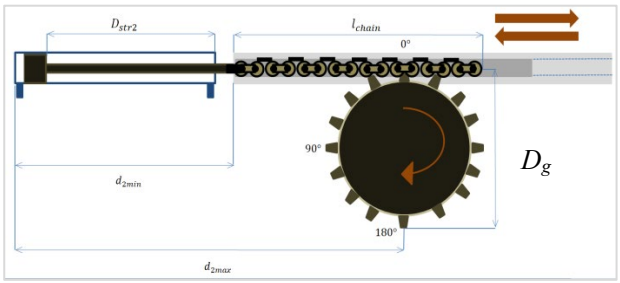

Fig. 8: Dimension calculation model for converting linear motion of actuator 2 into rotational motion.

By installing a block parallel to the piston pillar, the guiding cylinder enhances the carrying capacity of weights by stopping the piston from turning because of the guide pillar's added support. This is crucial when a system has to have extremely precise regulated linear motion or is subjected to heavy side stresses. Gear circumference $= \pi \times D_g = \pi \times 90 = 282.7$ mm.To achieve rotation of the panel at 180°, only half a cycle is needed in the movement. So the circumference of the circle must be divided by two; 282.7/2 = 141.37 mm ≈150 mm. Therefore, the stroke length of the piston cylinder (Actuator 2) $= D_{str2}$ = 150 mm.

2.5 Designing the cylinder internal diameter of the pneumatic actuator 2

After designing the stroke length of the pneumatic actuator 2, which allows the tracker to be moved 180°, the internal diameter of the cylinder of actuator 2 must be designed. Figure 9 shows the transition stages of actuator 2.

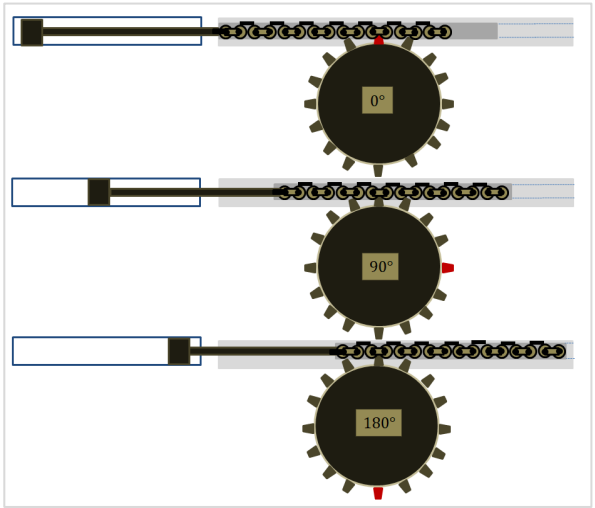

Fig. 9: Transition stages of actuator 2.

Heavy lateral loads require more planning because cylinders are primarily made to push and draw weights. Consideration should be given to designing the cylinder thrust to remain as near to the piston rod's centerline as feasible. When selecting the kind of cylinder and size of the piston, the main factor is the load. The weight of the solar panel is 4 kg, while the total weight of the structure with frame, pillar, and gear is about 0.65 kg, and the weight of the pneumatic cylinder 1 is 0.35 kg, so the total weight is about 5 kg.

$$F = [M \times g]_{int\ load} + [\frac{1}{2} \times \rho \times V^2 \times A_w \times C_d]_{wind\ load} \quad (12)$$

Wind load generates additional force that obstructs the movement of the actuator cylinder 2. There are two areas with an important impact facing the movement of the wind, including the solar panel and the side area of the pillar. The maximum effect of wind on the lateral area of the cross-section of the pillar (A_{pillar}) carrying the solar panel is added to the effect of the panel area A_p in Eq. 12 within the total wind effect area A_w as follows:

$$A_{panel} = a \times b = 0.67 \times 0.425 = 0.2848\ m^2$$

$$A_{pillar} = \frac{\text{Pillar circumference}}{2} \times \text{Pillar hight} = \frac{\pi D_p}{2} \times h = \frac{\pi \times 0.04}{2} \times 0.73 = 0.04584\ m^2.$$

The wind drag coefficient of the circular cross-section C_{d_piller} is equal to 0.47 while for the panel area C_{d_panel} is equal to 1.05 [40]. Since the effect of wind on the pneumatic actuators is very small, it has been neglected. Substituting the necessary values in Eq. 12 to get the maximum value of cylinder force in actuator 2:

$$F_{2(max)} = [M \times g]_{int\ load} + [\frac{1}{2} \times \rho \times V^2 \times (A_{panel} \times C_{d\_panel} + A_{pillar} \times C_{d\_piller})]_{wind\ load}$$

$$= [5 \times 9.81] + \left[\frac{1}{2} \times 1.29 \times 5.5^2 \times (0.2848 \times 1.05 + 0.04584 \times 0.47)\right] = 55.3\ kg\frac{m}{s^2} = 55.3\ N$$

At the tracking system's center of rotation, the torque of actuator 2 is determined by:

$$M_{act2} = F \times (l_{ch} + D_g) \quad (13)$$

Where l_{ch} is the length of the chain and D_g is the diameter of the gear. Substituting the values in Eq. 13 to get torque value as: $M_{act_2} = 59.171$ N. m.The tracking system's eccentric moment 2 is expressed as follows:

$$M_{e2} = m \times g \times \cos(\alpha) \times e \quad (14)$$

Figure 10 shows the plot of the tracking system's eccentric moment 2 as a function of angle α according to Eq. 14.

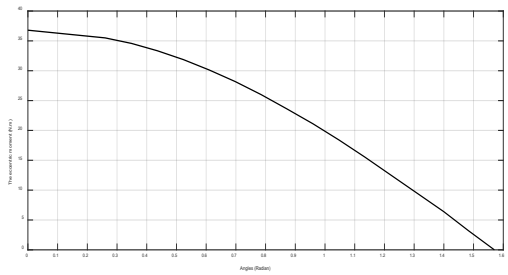

Fig. 10: Eccentric moment analysis of actuator 2 vs. angles.

The maximum value of the eccentric moment of the actuator 2 can be calculated by using $\alpha = 0^{o}$,

$$\mathrm{M_{e2_{(max)}}} = 5 \times 9.81 \cos(0) \times 0.750 = 36.7875 \text{ N.m}$$

The wind moment can be calculated as:

$$M_{wind} = C_m \times 0.613 \times V^2_{(wind)} \times A_w \times b \quad (15)$$

$$\mathrm{A_w} = \mathrm{A_{panel}} + \mathrm{A_{pillar}} = 0.2848 + 0.04584 = 0.33064 \text{ m}^2$$

By substituting the values in Eq. 15,

$$\mathrm{M_{wind}} = 0.6 \times 0.613 \times 5.5^2 \times 0.33064 \times 0.02 = 0.07356 \text{ N.m}$$

The torque balance M_{bal} equation can be given as:

$$M_{bal} = M_{act2} - M_{e2} - M_{wind} \quad (16)$$

Substituting the given values in Eq. 16, the torque balance $M_{bal} = 22.31$ N.m

The available force is the product of the cylinder's air pressure and piston area (force factor). The value of the force is 55.3 N and the air pressure in the system is constant at 2 bar. So the unknown value in the following force equation is the diameter area of the pneumatic actuator 2:

$$F_2 = P \times A_2 \quad (17)$$

Where A_2 is the area of cylinder 2. Substituting the values of force and pressure in Eq. 17 to get the actuator area $A_2 = 2.765 \times 10^{-4}\ m^2$.

It is known that,

$$A_2 = \frac{\pi}{4} \times {D_2}^2 \quad (18)$$

Where D_2 is the cylinder diameter of actuator 2. From Eq. 18, D_2 = 18.76 mm

The cylinder must be designed to avoid the influence of circumferential and hoop pressures, which may lead to bursting of the cylinder walls. To overcome these factors, the thickness of the cylinder wall must be sufficient to withstand the pressures created by the internal pressure of the air. This can be accomplished by choosing a safety factor of 1.5. So the diameter of the pneumatic cylinder (actuator 2) = 18.76 mm × 1.5 = 28.15 mm.

As seen in Fig. 3, the three roller bearings for this system correspond to the positions O, A', and B'. In this instance, the friction torque on standard roller bearings can be disregarded because it is extremely modest about the whole torque. Also, the bearings of the gear are neglected because the shaft is in the vertical direction as shown in Fig. 2. All previously designed system specifications and dimensions for the pneumatic actuators are tabulated in Table 1.

Table 1. Dimensions of pneumatic actuators

Dimensions (mm)	**Pneumatic actuator 1**	**Pneumatic actuator 2**
Cylinder stroke length	150	150
Cylinder internal diameter	22	28.15
Cylinder fully extended length	390	400
Cylinder fully retracted length	240	250
Chain length	-	170
Gear diameter	-	90

The design of the pneumatic actuator type might be aided by the actuator's size and force design. In this study, the pneumatic cylinders of the solar tracking system may be chosen for practical applications with the following specifications listed in Table 2.

Table 2. Practical specifications of pneumatic actuators

Item	Quantity	Specifications
Pneumatic cylinder	2	EXP- FLEX-MAC 30×150-S-0.05-1.0 Mpa with stroke of 150 mm The force (Max load) cylinder output 350 N, cylinder return force 307N, full retraction (240 ~ 250 mm) length & full extension (390~ 400 mm) length was chosen
Valves	4	3 Way 2 Position Normally closed Solenoid valve model: 3V210-08, Pressure 0.15-0.8Mpa input voltage 24VDC, 4.8W, port size 1/4 inch

3. Simulation Results and Discussion

Most of the relevant studies did not focus on the design process for the appropriate actuator size for the proposed application and according to climatic conditions, different loads, and other parameters. The design of the two pneumatic actuators for driving the solar tracker was simulated using MATLAB Software.

The simulation was conducted for 24 hours during the

day on 1st March 2024, in Baghdad, Iraq. The following data show additional information about timings: Dawn: 06:05:26, Sunrise: 06:30:02, Culmination: 12:14:38, Sunset: 17:59:43, Latitude: N 33°20'26.15"33.34060°, and Longitude: E 44°24'3.24"44.40090° [46]. Coordinates: 38S 444250 3689207, considering that the solar declination (δ) = -5.6785° [47]. In Fig. 11, the angles of azimuth and altitude in Baghdad are shown. Where the azimuth angle is considered as the input signal to the pneumatic actuator 2, whose movement is 180°, a daily movement. The altitude signal is considered an input signal to the pneumatic actuator 1, which follows the sun from south to north and is a seasonal movement. Fig. 12 shows the solar radiation in Baghdad during the day.

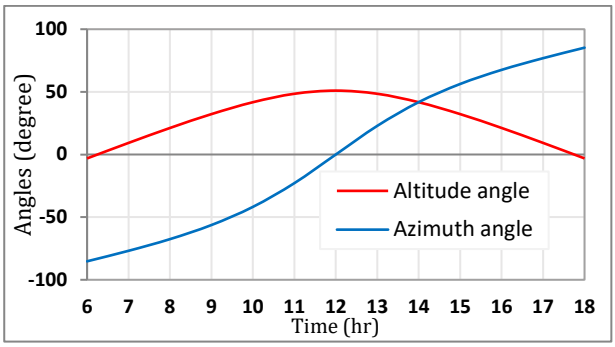

Fig. 11: Azimuth and Altitude angles during the day on the 1st day of March 2024.

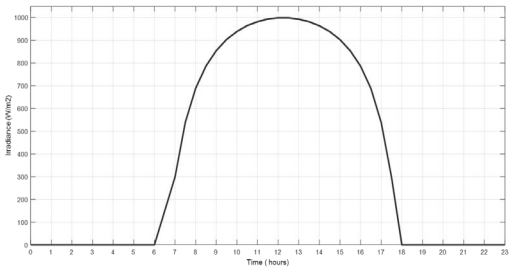

Fig. 12: Solar radiation during the day.

The stroke displacement of the pneumatic cylinder of actuator 1 during the day is shown in Fig. 13. The actuator starts working at 06:30 and ends at 17:30. While the simulation in Fig. 14 shows the position of actuator 2, which starts working at 6:00 and ends at 17:30.

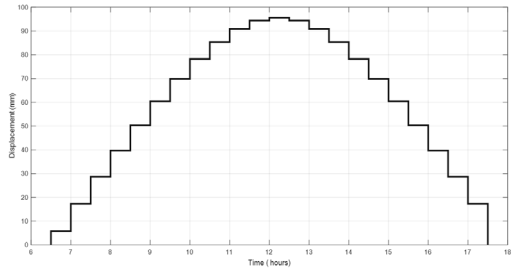

Fig. 13: Stroke displacement of the pneumatic actuator 1.

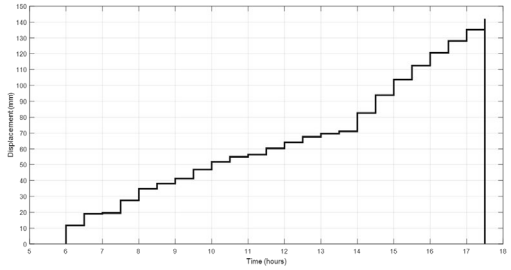

Fig. 14: Stroke displacement of the pneumatic actuator 2.

Figs. 15 and 16 show the scanning angles of the movement of solar panels in the vertical and horizontal planes during the day, respectively It can be noticed that the panel begins to move vertically at 06:30 and ends at 17:30 with a scanning angle of 0.89 rad (51°), while moving horizontally starting at 6:00 and ending at 17:30 with scanning angle of 2.9758 rad (170.5°). It is noted in Fig. 15 that the curve of the tracker angle rises in the morning until it reaches its peak at noon, at which point, the angle between the actuator 1 and the panel is 0.89 rad, after which the curve descends to the bottom at sunset. On the other hand, it is noted from Fig. 16 that the pneumatic cylinder 2, whose linear motion was converted into a rotary motion using a gear, has a gradual movement from an angle of 0.2 rad (11.46º) at 6:00 and continues to rise until it reaches the end of the cylinder stroke at an angle of 2.9758 rad (170.5º) at 17:30.

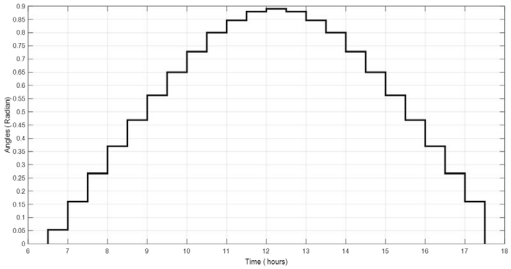

Fig. 15: Vertical scanning angles of the solar panel with actuator 1.

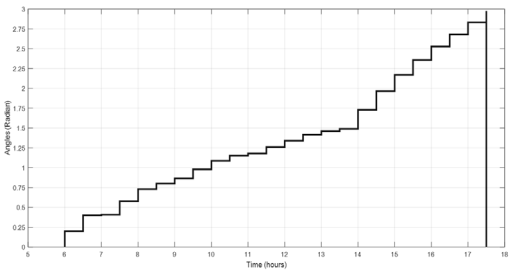

Fig. 16: Horizontal scanning angles of the solar panel with actuator 2.

By multiplying the output voltage and current of the solar panel while it is loaded with a 50 Ω resistance, one may calculate the output power (P_o) of the panel. Fig. 17 shows the output power curves for both a fixed PV panel and another situation in which the panel tracks the sun. It

is discovered that a mobile solar panel equipped with a tracking system generates an average power of 25.05 W, whereas a stationary solar panel generates an average of 15.05 W.

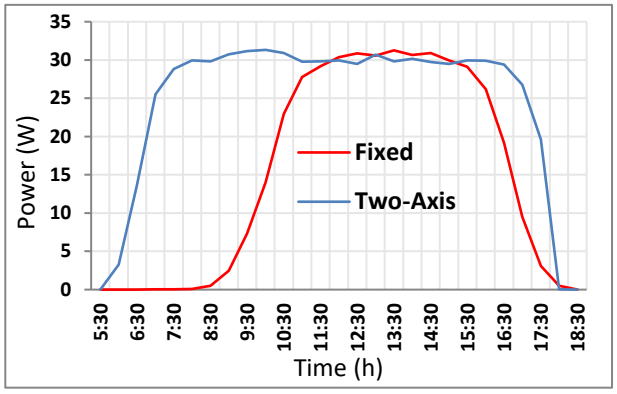

Fig. 17: PV panel output power during the day.

The figure illustrates how the power from the stationary panel rises steadily from sunrise to midday, when it reaches a value of 31.26 W, and then falls to its lowest value at sunset. In contrast, the power from the moving panel stays roughly at the level of 19 W from 7:30 until 16:30. Subsequently, it steadily drops until it reaches its lowest value at 18:30.

As illustrated in Fig. 18, the efficiency curves of a stationary or moving PV panel with respect to the sun's position can be drawn using the panel's area (A_p = 670×425 m^2), radiation intensity (G) curve (Fig. 12), and panel wattage curves (Fig. 17) that emerge from the panel. [17] states that efficiency may be assessed as follows:

$$\eta(\%) = \frac{P_o}{G A_p} \times 100\% \qquad (19)$$

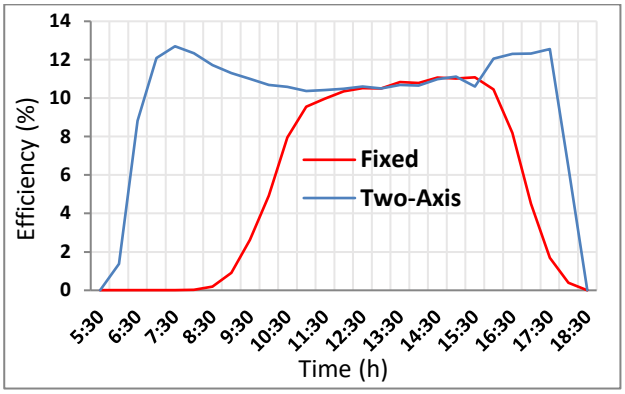

Fig. 18: PV panel efficiency during the day.

It is evident that throughout the day, the mobile panel's efficiency surpasses that of the stationary panel. The movable panel's efficiency is at its peak (12.7%) in the presence of sunlight. After that, it begins to decline until midday and then rises once again until dusk. When it comes to fixed panels, the situation is the exact reverse. The average efficiency of the moving panel is determined to be 8.8%, whereas that of the stationary panel is 5.287 %. This indicates that as compared to the stationary solar panel, the pneumatic tracking system increased the solar panel's efficiency by 66.4%.

4. Conclusions

The study offers a simple and comprehensive design approach that relies on a combination of factors such as tilt angle, actuator distance, torque, and pneumatic actuator power to drive a two-axis tracking system adapted to Iraq's climate. The design includes the inner diameter and length of the piston cylinder of the pneumatic actuators and its rotational control unit on an ordinary bright day, on the first of March 2024 in the city of Baghdad, the capital of Iraq. Using MATLAB software, the test results showed that the tracking system works accurately and stably and moves smoothly when loaded under the maximum wind speed that can occur, which is about 5.5 m/s according to Iraqi climate statistics. It was found that the length of the pneumatic cylinder is 150 mm for both pneumatic actuators. Also, it was found that the diameter area of the pneumatic cylinder of actuator 1 was 22 mm while it was 28.15 mm for actuator 2, taking into account the constant inlet pressure value of pneumatic actuators at 2 bar. The outcomes also shown that, in comparison to a fixed panel, the efficiency of the solar panel rose by 66.4% when it was orientated in two axes with pneumatic actuators.

The pneumatic actuator design procedures presented in this paper serve as a general guide that can be adopted by future research in the field of tracking systems driven by any type of actuator. It would be interesting to design hydraulic actuators that meet the same specifications as the proposed pneumatic tracking system and perform a comparative analysis with it.

Acknowledgments

My sincere appreciation goes out to the research supervisors, Dr. J.A.-K. Mohammed and Dr. W.E. Abdul-Lateef, for their direction, fervent support, and helpful critique of this study. I also appreciate Eng. Emad N. Abed for his support and advice

Nomenclature

A_1, A_2	Area of cylinders 1 & 2 (m^2)
A_p	Solar panel area (m^2)
A_{pillar}	Pillar cross-section (m^2)
A_w	Area of moving parts exposed to wind (m^2)
b	Solar panel width relative to rotation axis (m)
C_d	Wind drag coefficient (-)
C_m	Wind moment coefficient (-)

D_a	Actuator diameter (m)
D_g	Gear diameter (m)
D_p	Pillar diameter (m)
D_{str}	Actuator stroke length (m^2)
d_{max}	Fully extended length (m)
d_{min}	Fully retracted length (m)
e	Eccentricity (m)
F	Force (N)
g	Acceleration due to gravity (m/s^2)
h	Pillar height (m)
l_{ch}	Chain length (m)
M	Mass of moving components of tracker (kg)
M_{wind}	Wind moment concerning the system's rotational axis (N.m)
M_{bal}	Torque balance of the rotation system (N.m)
M_{act}	Actuator torque at the tracker's center of rotation (N.m)
M_e	Eccentric moment of tracking system (N.m)
m	Solar panel weight (kg)
P	Air pressure (bar)
V	Wind speed (m/s)
α	Solar panel angle with vertical axis (radian)
ρ	Density of air (kg/m^3)

References

1) P.A. Owusu, S.A.-Sarkodie, S. Dubey, "A review of renewable energy sources, sustainability issues and climate change mitigation", *Cogent Eng.*, 3 (1) (2016) 1167990. https://doi.org/10.1080/23311916.2016.1167990
2) Y.-D. Kim, K. Thu, K.C. Ng, Evaluation and parametric optimization of the thermal performance and cost effectiveness of active-indirect solar hot water plants, *Evergreen* 2 (2) 50-60 (2015). https://doi.org/10.5109/1544080
3) K. Tewari, R. Dev, "Analysis of modified solar water heating system made of transparent tubes & insulated metal absorber," *Evergreen* 5 (1) 62-72 (2018). https://doi.org/10.5109/1929731
4) A.A. Ismaeel, H.A.A. Wahhab, Z.H. Naji, "Performance evaluation of updraft air tower power plant integrated with double skin solar air heater", *Evergreen* 8 (2) 296–303 (2021). https://doi.org/10.5109/4480706
5) R. Kumar, S.K. Verma, N.K. Gupta, S.K. Singh, "Performance Enhancement of TSAH using Graphene and Graphene/CeO2-Black Paint Coating on Absorber: A Comparative Study," *Evergreen* 9 (3) 673-681 (2022). https://doi.org/10.5109/4843098
6) L.A. Rasheed, J.A.-K. Mohammed, R.A. Jessam, "Performance Enhancement of a Single Pass Solar Air Heater by Adopting Wire Mesh Absorber Layer," *Evergreen*, 10 (2) 880-887 (2023). https://doi.org/10.5109/6792883
7) L.A. Rasheed, J.A.-K. Mohammed, R.A. Jessam, "Performance Enhancement of Solar Air Heater by Integrating Innovative Absorber Design and Automatic Control Flow Rate," *Evergreen*, 10 (3) 1439-1448 (2023). https://doi.org/10.5109/7151693
8) L.A. Rasheed, A.V. Yurchenko, V.I. Syryamkin, J.A.-K. Mohammed, "OPTIMIZATION OF AGRICULTURAL DRYING USING PCM BASED AUTOMATED INDIRECT SOLAR DRYERS," *Russian Physics Journal*, 66 (9) 983-989 (2023). https://doi.org/10.1007/s11182-023-03033-9
9) O.A. Towoju, O.A. Oladele, "Electricity Generation from Hydro, Wind, Solar and the Environment", *Eng. and Tech. J.,* 39, (9) 1392-1398 (2021). https://doi.org/10.30684/etj.v i9.2145
10) B. Belgasim, Y. Aldali, M.J.R. Abdunnabi, G. Hashem, K. Hossin, "The potential of concentrating solar power (CSP) for electricity generation in Libya," Renew. *Sustain. Energy Rev.* (90) 1-15 (2018). https://doi.org/10.1016/j.rser.2018.03.045
11) A. Musa, E. Alozie, S.A. Suleiman, J.A. Ojo, A.L. Imoize, "A Photovoltaic Tracking Systems", *Information*, 14 (4) 211 (2023). https://doi.org/10.3390/info14040211
12) Awasthi, A., Shukla, A.K., Manohar, M.S.R., Dondariya, C., Shukla, K.N., Porwal, D., Richhariya, G. Review on Sun Tracking Technology in Solar PV System. *Energy Rep*. (6) 392–405 (2020). https://doi.org/10.1016/j.egyr.2020.02.004
13) S. Mirić, R. Giuffrida, G. Rohner, D. Bortis, J.W. Kolar, "Design and Experimental Analysis of a Selfbearing Double-Stator Linear-Rotary Actuator", *IEEE Int. Elec. Mach. Drives Conf. (IEMDC)* (2021). https://doi.org/10.1109/IEMDC47953.2021.9449501
14) V.A. Kusuma, A.A. Firdaus, S.S. Suprapto, R.J. Yuniar, H. Trimulya, Y.T. K. Priyanto, "Comparative analysis of single-axis solar tracker performance with and without reflector under various weather conditions," *Int. J. Appl. Power Eng*. 13 (2) 328-334 (2024). https://doi.org/10.11591/ijape.v13.i2.pp328-334
15) V.S. Qader, O. M. Ali, N. I. Hasan, "An Experimental Comparison Between Fixed and Single-Axis Tracking Photovoltaic Solar Panel Performance: Zakho City as Case Study," *Al-Rafidain Eng. J.*, 28 (1) 272–279 (2023). https://doi.org/10.33899/rengj.2022.136292.1204
16) N. Thungsuk, T. Tanaram, A. Chaithanakulwat, T. Savangboon, A. Songruk, N. Mungkung, T.

Maneepen, S. Arunrungrusmi, W. Poonthong, N. Kasayapanand, "Performance Analysis of Solar Tracking Systems by Five-Position Angles with a Single Axis and Dual Axis," *Energies*, 16 (16) 5869 (2023). https://doi.org/10.3390/en16165869

17) F.M. Mohammed, J.A.-K. Mohammed, R.A. Nouri, "Efficiency Enhancement of a Dual-axis Solar PV Panel Tracker Using Water-Flow Double Glazing Technique," Al-Khwarizmi Eng. J. 14 (13) 32-47(2018). https://doi.org/10.22153/kej.2018.12.008
18) S.T. Hamidi, J.A.-K. Mohammed, L.M. Reda, "Design and Implementation of an Automatic Control for Two Axis Tracking System for Applications of Concentrated Solar Thermal Power," *Al-Khwarizmi Eng. J.* 14 (4) 54-63 (2018). https://doi.org/10.22153/kej.2018.01.010
19) H. Asyari, A.W. Aji, "Desain Solar Tracking Dual Axis Berbasis Arduino dan Sensor Light Dependent Resistor untuk Meningkatkan Daya Keluaran Sel Surya," *J. Tek. Elektro Uniba (JTE UNIBA)*, 7 (2) 320–324 (2023). https://doi.org/10.36277/jteuniba.v7i2.218
20 L. Halim, S. E. Gun, F. Wahab, "Solar Panel Efficiency Improvement through Dual-Axis Solar Tracking with Fuzzy Logic and Water Treatment Techniques," *J. Nas. Tek. Elektro*. 12(3) 20–29 (2023). https://doi.org/10.25077/jnte.v12n3.1120.2023
21) P. Muthukumar, S. Manikandan, R. Muniraj, T. Jarin, A. Sebi, "Energy efficient dual axis solar tracking system using IOT," *Meas. Sens*. 28 (100825) (2023). https://doi.org/10.1016/j.measen.2023.100825
22) K.J. Alaameri, A.J. Ramadhanand, A.S. Maklakov, "Design of dual-axis solar tracking system with integrated cleaning system: Case study of Najaf city, Iraq," in *AIP Conference Proceedings*, (2022). https://doi.org/10.1063/5.0066840
23) Shang, H., Shen, W. Design and Implementation of a Dual-Axis Solar Tracking System. *Energies*, 16, 6330 (2023). https://doi.org/10.3390/en16176330
24) A. Riad, M.B. Zohra, A. Alhamany, M. Mansouri , "Bio-sun tracker engineering self-driven by thermo-mechanical actuator for photovoltaic solar systems", *Case Stud. Therm. Eng.* 21, 100709 (2020). https://doi.org/10.1016/j.csite.2020.100709
25) X. Zhou, "Tracking and Analysing Error in Feedback Linearized Motion Trajectory of Hydraulic Actuator Based on the Internet of Things," *Mobile Information Systems*, 2022, ID 2195498. https://doi.org/10.1155/2022/2195498
26) S.G. Babu, "The Effect of a Pneumatic Cylinder-Based Solar Tracking System on the Electricity Production of a Photovoltaic Panel," (2022). *South Carolina Junior Academy of Science* 38. https://scholarexchange.furman.edu/scjas/2022/all/38
27) L. Born, E.A.G.S. Martín, M. Ridder, A.H. Körner, J. Knippers, G.T. Gresser, "FlectoSol – A pneumatically activable PV-functionalized façade shading module with bending motion in two directions for solar tracking," *Develop. in the Built Envir.*, 18 (2024) ID: 100372. https://doi.org/10.1016/j.dibe.2024.100372
28) J. Pustavrh, M. Hočevar, P. Podržaj, A. Trajkovski, F. Majdič, "Comparison of hydraulic, pneumatic and electric linear actuation systems", *Scientific Reports*, 13 (20938) (2023). https://doi.org/10.1038/s41598-023-47602-x
29) A.A. Mansour, W.M. Hashim, A.A.W. Muhammad, "Design and Implementation of a Pneumatic Servo System using Conventional Direction Control Valve," *IRAQI J. Comput. Com. Control Syst. Eng.*, 18 (3) 1–11 (2018). https://doi.org/10.33103/uot.ijccce.18.3.1
30) B. Okonkwo, M.C. Osuagwu, C.C. Chiabuotu, K.C. Aladum, "Design Analysis of a Pneumatic Vehicle", *J. of Basic and App. Res. Int.,* 29 (2) 1-15 (2023). https://doi.org/10.56557/JOBARI/2023/v29i28250
31) V.A. Atindana, X. Xu, A.N. Nyedeb, J.K. Quaisie, J.K. Nkrumah, S.P. Assam, "The Evolution of Vehicle Pneumatic Vibration Isolation: A Systematic Review," *Shock and Vibration* (2023). ID 1716615. https://doi.org/10.1155/2023/1716615
32) J.A.-K. Mohammed, H. Kareem, A. Sabeeh, "Implementation of an Electro-Pneumatic Prototype Elevator Controlled by PLC", *Eng. and Tech. J.,* 33 (8A) 1986-1998 (2015). https://doi.org/10.30684/etj.2015.108840
33) F.M. Mohammed, J.A.-K. Mohammed, M.A. Naji, "Implementation of an Automated Vacuum Elevator System", J. of Univ. of Babylon for Eng. Sci. 26 (10) 150-165(2018). https://www.journalofbabylon.com/index.php/JUBES/article/view/1810
34) T. Sénac, A. Lelevé, R. Moreau, C. Novales, L. Nouaille, M.T. Pham, P. Vieyres, "A Review of Pneumatic Actuators Used for the Design of Medical Simulators and Medical Tools," *Multimodal Technol. Interact* 3(3) 47 (2019). https://doi.org/10.3390/mti3030047
35) J. Walker, T. Zidek, C. Harbel, S. Yoon, F.S. Strickland, S. Kumar, M. Shin, "Soft robotics: A review of recent developments of pneumatic soft actuators," *Actuators* 9 (1) 3 (2020). https://doi.org/10.3390/act9010003
36) S. Ergashev, E. Oshchepkova, "Design of a dual axis solar tracking system with strong wind protection system," *BIO Web of Conferences* 84, 05032 (2024). https://doi.org/10.1051/bioconf/20248405032
37) R.R. Chaurasia, V.P. Ganpatil, S.S. Khule, N. Pawar, "Design And Development of Hydraulic Solar Tracking System," *Inter. J. Adv. Resear. and Innov.*

Ideas in Educ. (IJARIIE) 10 (2) (2024) 3937-3942.
38) B. Baisrum, B. Setiadi, S. Sudrajat, V. Wijayakusuma, H. Ulhaq, R. Hikmawati, N. Qamaruddin, S. Hardiansyah , "Implementation of Adaptive Neuro-Fuzzy Inference System Control on Pneumatic Solar Tracker," *Proc. of the 2nd Int. Semin. Scie. Appl. Tech. (ISSAT 2021)*, *Adv. in Eng. Resear*. 207 (2021) 422-429. https://doi.org/ 10.2991/aer.k.211106.067
39) T. Dhanya, P.M. Gopal, "Modeling and Design of Pneumatic Actuator System for Solar PV Tracking," Int. J. Mech. Eng. 7 (4) 201-206 (2022).
40) M. Fathi, R. Amjadifard, F. Eshghi, M. Kelarestaghi, "Design and implementation of a novel multi-faceted-efficient pneumatic dual-axis solar tracker", *World J. of Eng*., 21 (2) (2024) 254-266. https://doi.org/10.1108/WJE-04-2022-0173
41) H.Q. Adeeb, Y.K. Al-Timimi, "GIS techniques for mapping of wind speed over Iraq," *Iraqi J. Agric. Sci.,* 50 (6) (2019). https://doi.org/10.36103/ijas.v50i6.852
42) A.K. Mishaal, A.M. Abd Ali, A.B. Khamees, "Wind Distribution Map of Iraq-A Comparative Study," in *IOP Conf. Ser.: Mater. Sci. Eng.* 928 (2020), 022044. https://doi.org/10.1088/1757-899X/928/2/022044
43) M. Bashaer, O.I. Abdullah, A. Al-Tmimi, "Investigation and analysis of wind turbines optimal locations and performance in Iraq," *FME Trans.*, 48 (2) 155–163 (2020). https://doi.org/10.5937/fmet2001155B
44) A.H. Mahdi, "Statistical Distributions of Wind Speed for Baghdad, Basra and Mosul Governorates", *Eng. and Tech. J.,* 31 (4A) (2013) 752-773. https://doi.org/10.30684/etj.31.4A.13
45) Z. Gao, S. Zhou, J. Zhang, Z. Zeng, X. Bi. Parameterization of Sea Surface Drag Coefficient for All Wind Regimes Using 11 Aircraft Eddy-Covariance Measurement Databases. *Atmosphere*. 12 (1485) (2021). https://doi.org/10.3390/atmos12111485
46) F.I. Mustafa, A.S. Al-Ammri, F.F. Ahmad, "Direct and indirect sensing two-axis solar tracking system," *in 2017 8th Int. Ren. En. Cong. (IREC), IEEE,* (2017) 1–4. https://doi.org/10.1109/IREC.2017.7926026
47) F.I. Mustafa, S. Shakir, F.F. Mustafa, A.T. Naiyf, "Simple design and implementation of solar tracking system two axis with four sensors for Baghdad city," in *2018* IEEE *9th Int. Ren. En. Cong. (IREC)*. (2018) 1–5. https://doi.org/10.1109/IREC.2018.8362577